Computational Materials Science 81 (2014) 216–225

Contents lists available at ScienceDirect

Computational Materials Science

journal homepage: www.elsevier.com/locate/commatsci

Physical, mathematical, and numerical derivations of the Cahn–Hilliard equation

Dongsun Lee [a], Joo-Youl Huh [b], Darae Jeong [a], Jaemin Shin [a], Ana Yun [a], Junseok Kim [a,*]

[a] Department of Mathematics, Korea University, Seoul 136-713, Republic of Korea
[b] Department of Materials Science and Engineering, Korea University, Seoul 137-713, Republic of Korea

ARTICLE INFO

Article history:
Received 19 June 2013
Received in revised form 9 August 2013
Accepted 12 August 2013
Available online 14 September 2013

Keywords:
Chemical processes
Mathematical modeling
Numerical analysis
Phase change
Cahn–Hilliard
Pseudospectral method

ABSTRACT

We review physical, mathematical, and numerical derivations of the binary Cahn–Hilliard equation (after John W. Cahn and John E. Hilliard). The phase separation is described by the equation whereby a binary mixture spontaneously separates into two domains rich in individual components. First, we describe the physical derivation from the basic thermodynamics. The free energy of the volume Ω of an isotropic system is given by $N_V \int_\Omega [F(c) + 0.5\epsilon^2 |\nabla c|^2] d\mathbf{x}$, where N_V, c, $F(c)$, ϵ, and ∇c represent the number of molecules per unit volume, composition, free energy per molecule of a homogenous system, gradient energy coefficient related to the interfacial energy, and composition gradient, respectively. We define the chemical potential as the variational derivative of the total energy, and its flux as the minus gradient of the potential. Using the usual continuity equation, we obtain the Cahn–Hilliard equation. Second, we outline the mathematical derivation of the Cahn–Hilliard equation. The approach originates from the free energy functional and its justification of the functional in the Hilbert space. After calculating the gradient, we obtain the Cahn–Hilliard equation as a gradient flow. Third, various aspects are introduced using numerical methods such as the finite difference, finite element, and spectral methods. We also provide a short MATLAB program code for the Cahn–Hilliard equation using a pseudospectral method.

© 2013 Elsevier B.V. All rights reserved.

1. Introduction

In this paper, we review physical, mathematical, and numerical derivations for the binary Cahn–Hilliard (CH) equation, and we provide a short MATLAB program code for the equation using a pseudospectral method. The CH equation describes the temporal evolution of a conserved field that is a continuous, sufficiently differentiable function of position. The evolution of the phase separation is due to the non-Fickian diffusion driven by gradients in chemical potential. It was originally proposed to model the spinodal decomposition of a binary A–B system at a fixed temperature, for which an initially homogeneous system with a uniform composition of c, the mole fraction of component B, spontaneously decomposes into two phases with the same crystal structure, but with different compositions. In this case, the spatial distribution of the two phases during decomposition could be described by the composition field, $c(\mathbf{x}, t)$, which is a continuous, differentiable function of position ($\mathbf{x}$) and time (t) [1]. The temporal evolution of the spinodal decomposition in the system is governed by the CH equation [2]:

$$\frac{\partial c}{\partial t} = \nabla \cdot (M \nabla \mu) = M \Delta \mu, \tag{1}$$

where M is the constant mobility. In general, M is the tensor-valued variable mobility [3]. Here μ is the local chemical potential defined as

$$\mu = F'(c) - \kappa \Delta c. \tag{2}$$

In Eq. (2), $F(c)$ is the Helmholtz free energy density per molecule of the homogeneous system with composition c, and κ is a positive constant often called the gradient energy coefficient ($\kappa = \epsilon^2$), which is related to the interfacial energy.

The essential concept underlying the CH equation is that the interface between two phases, say α and β phases, is not sharp, but has a finite thickness in which the composition c changes gradually. For instance, when the binary system approaches near the equilibrium state composed of α phase with $c = c_\alpha^{eq}$ and β phase with $c = c_\beta^{eq} > c_\alpha^{eq}$, the domains where $c(\mathbf{x}, t) = c_\alpha^{eq}$ and $c(\mathbf{x}, t) = c_\beta^{eq}$ correspond to the α and β phases, respectively, whereas the region where $c(\mathbf{x}, t)$ varies gradually from c_α^{eq} to c_β^{eq} represents the interface between the α and β phases, as shown in Fig. 1.

One of the most striking advantages of using the CH equation for simulating microstructural evolution is the avoidance of explicit tracking of the interface. This concept of a diffuse interface has been adopted to model various physical phenomena involving

* Corresponding author. Tel.: +82 2 3290 3077; fax: +82 2 929 8562.
E-mail address: cfdkim@korea.ac.kr (J. Kim).
URL: http://math.korea.ac.kr/~cfdkim (J. Kim).

0927-0256/$ - see front matter © 2013 Elsevier B.V. All rights reserved.
http://dx.doi.org/10.1016/j.commatsci.2013.08.027

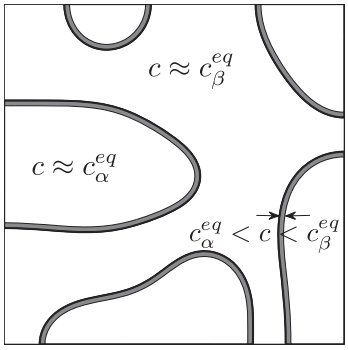

Fig. 1. Two phase microstructure with order parameter c.

moving interfaces, in which the order parameter, or phase field $\phi(\mathbf{x}, t)$, instead of the composition field $c(\mathbf{x}, t)$, is introduced to describe the spatial distribution of the entire microstructure of a system. If the overall phase fraction in the system is conserved during evolution, as in the coarsening phenomenon of a precipitate phase in a matrix phase, the governing equation for the temporal equation of $\phi(\mathbf{x}, t)$ is given by a CH-type equation similar to Eq. (1).

Some examples of applications of the CH equation are the phase separation of binary and ternary liquid mixture [4,5], multi-phase fluid flows [6–9], Taylor flow in mini/microchannels [10], two-layer flow in channels with sharp topographical features [11], spinodal decomposition with composition-dependent heat conductivities [12], phase decomposition and coarsening in solder balls [13], the thermal-induced phase separation phenomenon [14], the evolution of arbitrary morphologies and complex microstructures such as solidification, solid-state structural phase transformations [15–18], meta-stable chemical composition modulations in the spinodal region [19], modeling of martensitic phase transformation [20], grain growth [21], pore migration in a temperature gradient [22], image inpainting [23,24], and tumor growth [25,26].

The remainder of this paper is organized as follows. Section 2 describes a detailed physical derivation of the CH equation using basic thermodynamics. Section 3 reviews a mathematical derivation of the CH equation as a gradient flow and mathematical analysis of the equation. Section 4 presents several numerical methods up to now for solving the CH equation. Finally, Section 5 states the conclusions.

2. Physical derivation

In this section, the CH equation is derived along the lines of some previous studies [1,27,28] by using basic thermodynamics. Considering a binary, regular solid solution at constant temperature, we first derive the form of the Helmholtz free energy density, $F(c)$, for a homogeneous system. Then, we derive the local free energy density for a compositionally inhomogeneous system, so as to obtain the total free energy of an inhomogeneous system having volume V, with F as a functional of $c(\mathbf{x}, t)$. The local chemical potential, μ, which must be uniform throughout the system in equilibrium, is defined as the variational derivative of F and the mass flux $\mathcal{J}$ is proportional to the minus gradient of μ. Finally, the CH equation is obtained by substituting the constitutive equation between $\mathcal{J}$ and μ into the continuity equation for mass conservation. We denote the free energy of a domain bounded by Ω in $\mathbb{R}^d$ $(d = 1, 2, 3)$, as $N_V \int_\Omega [F(c) + 0.5\epsilon^2 |\nabla c|^2] d\mathbf{x}$. Using the usual continuity equation, we obtain the CH equation. A detailed descriptions is provided below. The following derivations have been obtained in previous studies [1,27,28]. First, we derive the form of $F(c)$, the free energy per molecule of a homogenous system.

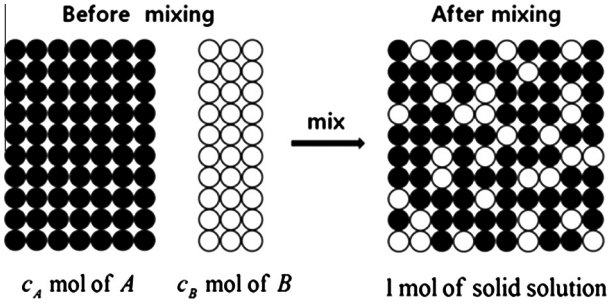

Fig. 2. Free energy of mixing. Before mixing: $F^0 = c_A F_A^0 + c_B F_B^0$, after mixing: $F_{mix} = F^0 + \Delta F_{mix}$.

2.1. Free energy of a homogeneous system

For a simple and closed system to be in equilibrium at fixed temperature (T) and volume (V), its Helmholtz free energy F must be minimized. By definition, the Helmholtz free energy of a system, F, is given by $F = E - TS$, where E and S are the internal energy and entropy of the system, respectively. In general, the thermodynamic properties of a solid solution will include a combination of its configurational, vibrational, electronic, and magnetic properties. For example, consider the process for preparing a binary A–B solid solution by mixing pure A and B at a fixed temperature. This mixing process will, in principle, result in not only configurational and vibrational changes, but also electronic and magnetic changes in each atom. For simplicity, by assuming that pure A and B have an equal molar volume and exhibit no changes in molar volume when mixed, only the configurational contributions will be taken into account for investigating the changes in thermodynamic properties during the mixing process.

Consider one mole of a binary solid system composed of N_A atoms of A and N_B atoms of B. The overall composition of the system is given by the mole fraction of component B, c, defined as $c = N_B/(N_A + N_B) = N_B/N_a$, where N_a is Avogadro's number (6.023×10^{23}). When the N_A atoms of A and N_B atoms of B are randomly mixed at a fixed temperature T, the binary solid mixture is a homogenous solid solution with a uniform composition c. Thus, we consider the homogenous solid solution as a regular solution, assuming random mixing of components A and B while accounting for the difference in the chemical affinity between A and B from those between atoms of the same type. In order to obtain the molar Helmholtz free energy of the regular solution, as shown in Fig. 2, consider the isothermal mixing process of $1 - c$ moles of pure A and c moles of pure B. The molar Helmholtz free energy of the system before mixing, F^0, is the weighted sum of those of the pure components, F_A^0 and F_B^0, and is given by $F^0 = E^0 - TS^0 = (1 - c)F_A^0 + cF_B^0$, as shown in Fig. 3. The mixing process alters the atomic configuration of A and B in the system, leading to changes in the internal energy and entropy, i.e., ΔE_{mix} and

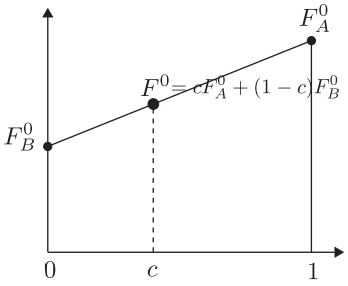

Fig. 3. Variation in the free energy F^0 before mixing with alloy composition c.

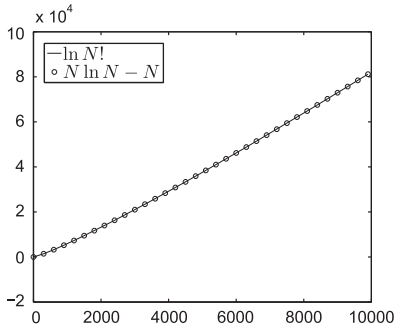

Fig. 4. Plots of $\ln N!$ and $N\ln N - N$.

ΔS_{mix}, respectively. Therefore, the molar Helmholtz free energy of the system after mixing, F_{mix}, can be expressed as

$$F_{mix} = F^0 + \Delta F_{mix}, \tag{3}$$

where $\Delta F_{mix} = \Delta E_{mix} - T\Delta S_{mix}$ is the molar Helmholtz free energy of mixing.

The mixing or configurational entropy, ΔS_{mix}, can be obtained from the Boltzmann equation

$$\Delta S_{mix} = k \ln \frac{W_{mix}}{W^0}, \tag{4}$$

where k is Boltzmann's constant, W^0 and W_{mix} are the numbers of ways in which the N_A atoms of A and N_B atoms of B can be arranged before and after mixing, respectively. Since atoms of a given type are indistinguishable, $W^0 = 1$, and in the case of random mixing, $W_{mix} = N_a!/(N_A!N_B!)$. Therefore, the molar entropy change due to random mixing of pure A and B is given by $\Delta S_{mix} = k\ln[N_a!/(N_A!N_B!)]$.

Applying Stirling's approximation ($\ln N! \approx N\ln N - N$ for large N, also see Fig. 4), the molar entropy change in the formation of a homogeneous solution with composition c is obtained as

$$\begin{aligned}\Delta S_{mix} &= k(N_a \ln N_a - N_A \ln N_A - N_B \ln N_B) \\ &= -R[(1-c)\ln(1-c) + c\ln c],\end{aligned}$$

where $R = kN_a$ is the universal gas constant. It is noted that ΔS_{mix} becomes zero when $c = 0$ (pure A) or $c = 1$ (pure B), and is positive otherwise. For the internal energy change ΔE_{mix} associated with the configurational change due to mixing, we again consider a randomly mixed solution of the N_A atoms of A and N_B atoms of B; then, we calculate its internal energy E_{mix} as the pairwise sum of interatomic potentials for each atom in the solution. Although the interactions among atoms over solids can occur in a long range, for simplicity, only the pairwise interaction among the nearest neighboring atoms will be taken into account herein. Let ϵ_{AA}, ϵ_{BB}, and ϵ_{AB} be the interaction potentials of A–A, B–B, and A–B bonds, respectively. By taking the relative zero of potential as that when two atoms are infinitely far apart, the pairwise potentials ϵ_{AA}, ϵ_{BB}, and ϵ_{AB} are negative quantities. Then, E can be expressed as

$$E = P_{AA}\epsilon_{AA} + P_{BB}\epsilon_{BB} + P_{AB}\epsilon_{AB}, \tag{5}$$

where P_{AA}, P_{BB}, and P_{AB} represent the numbers of A–A, B–B, and A–B bonds in the system, respectively. If each atom in the solid system has z nearest neighbors, the numbers of pairwise bonds associated with the N_A atoms of A and N_B atoms of B are related to P_{AA}, P_{BB}, and P_{AB} as $N_Az = P_{AB} + 2P_{AA}$ and $N_Bz = P_{AB} + 2P_{BB}$, respectively. Therefore, P_{AA} and P_{BB} can be expressed, respectively, as

$$P_{AA} = \frac{N_Az}{2} - \frac{P_{AB}}{2} \quad \text{and} \quad P_{BB} = \frac{N_Bz}{2} - \frac{P_{AB}}{2}. \tag{6}$$

Substituting Eq. (6) into Eq. (5) gives

$$E = \left[\frac{N_Az}{2}\epsilon_{AA} + \frac{N_Bz}{2}\epsilon_{BB}\right] + P_{AB}\left[\epsilon_{AB} - \frac{1}{2}(\epsilon_{AA} + \epsilon_{BB})\right]. \tag{7}$$

It is easily seen that the first term, i.e., the leading square bracket on the right-hand side of Eq. (7), corresponds to the internal energies of pure A and B before mixing. Therefore, the second term on the right-hand side of Eq. (7) represents the change in internal energy due to mixing, ΔE_{mix}.

Now, consider P_{AB} in the case of random mixing where the probabilities for a lattice site to be occupied by A and B are $1 - c$ and c, respectively. There are $N_az/2$ pairwise bonds in one mole of the solid solution, and the probability for each bond to be an A–B bond is $2c(1 - c)$, leading to $P_{AB} = z\,N_ac(1 - c)$. Therefore, in the case of random mixing, the molar internal energy change of mixing is given by

$$\Delta E_{mix} = zN_ac(1-c)\left[\epsilon_{AB} - \frac{1}{2}(\epsilon_{AA} + \epsilon_{BB})\right] = \Omega c(1-c), \tag{8}$$

where $\Omega = z\,N_a[\epsilon_{AB} - (\epsilon_{AA} + \epsilon_{BB})/2]$ is often called the regular solution constant, assuming the pairwise interaction potentials to be independent of temperature. When $c = 0$ or $c = 1$, ΔE_{mix} becomes zero as expected. Otherwise, ΔE_{mix} is either positive or negative depending on the sign of Ω. For instance, if $|\epsilon_{AB}| < |\epsilon_{AA} + \epsilon_{BB}|/2$, Ω is positive, and thus, ΔE_{mix} becomes positive.

Using Eqs. (5) and (8), the molar Helmholtz free energy of mixing, ΔF_{mix} in Eq. (3), is expressed as a function of T and c:

$$\Delta F_{mix}(T,c) = \Omega c(1-c) + RT[(1-c)\ln(1-c) + c\ln c]. \tag{9}$$

Since the thermodynamics is primarily concerned with changes in thermodynamic properties and not their absolute values, $\Delta F_{mix}(T, c)$ expressed by Eq. (9) can equivalently be used as the molar Helmholtz free energy of the regular solution, $F(T, c)$, which is measured with respect to the reference $F^0(T, c)$. Therefore, the Helmholtz free energy density per atom (or molecule) of a binary regular solution can be expressed as

$$\begin{aligned}F(T,c) &= \frac{\Delta F_{mix}}{N_a} \\ &= \frac{1}{N_a}\{\Omega c(1-c) + RT[(1-c)\ln(1-c) + c\ln c]\}.\end{aligned} \tag{10}$$

Fig. 5 shows the plots of $\Delta F_{mix}(T, c)$ depicted as a function of c at various temperatures in the case of $\Omega > 0$. When temperature is greater than the critical temperature $T_c = \Omega/2R$, free energy curve is plotted as a convex-downward function of c, implying that a homogeneous solution in the entire range of composition is stable against any compositional separation. However, when $T < T_c$, the free energy curve becomes convex upward in a certain composition range about $c = 0.5$. When the free energy of a homogeneous solution is located in the convex-upward part of the free energy curve, any small fluctuation in composition lowers the free energy

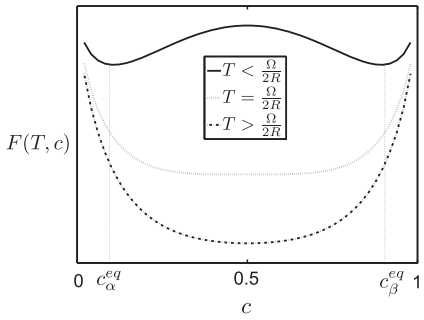

Fig. 5. Free energy as a function of the order parameter for different values of temperature.

and, thus, the homogeneous solution spontaneously evolves toward an $\alpha + \beta$ two-phase mixture with α and β phases having composition of c_α^{eq} and c_β^{eq}, respectively. The equilibrium compositions of α and β phases, $c = c_\alpha^{eq}$ and $c = c_\beta^{eq}$, correspond to the compositions that give the local minima of the free energy, as shown in Fig. 5. If the simple, closed system is subjected to fixed temperature (T) and pressure (P) as more often encountered in practice, the free energy to be minimized for equilibrium of the system is the Gibbs free energy G, rather than the Helmholtz free energy F, of the system. Herein, $G \equiv F - PV$ is also measured relative to the unmixed components as for F. When the mixing process does not involve a volume change as stipulated in the derivation of Eq. (10), G is equivalent to F. In general, when a simple system consisting of condensed phases such as liquids or solids is concerned, G of the system under ambient pressures can practically be treated as being equivalent to F of the system because the contribution of the PV term is negligible due to small molar volumes of condensed phases.

2.2. Free energy of a heterogeneous system

Next, we derive the general equation for the free energy of a nonuniform system having spatial variation in composition. Henceforth, let $F(c) = \Delta F_{\text{mix}}/N_a$. The total free energy of the volume Ω of an isotropic system with nonuniform composition is given by

$$\mathcal{E}(c) = N_V \int_\Omega \left[F(c) + \frac{\epsilon^2}{2}|\nabla c|^2\right] \mathrm{d}\mathbf{x}, \tag{11}$$

where N_V is the number of molecules per unit volume, ∇c is the composition gradient, F is the free energy per molecule of the homogeneous system, and ϵ is a parameter that is constant for a regular solution [1]. Let us review the derivation of the total free energy functional (11). First, we write the total free energy functional as

$$\mathcal{E}(c) = N_V \int_\Omega f \, \mathrm{d}\mathbf{x}, \tag{12}$$

where the local free energy per molecule, f, in a region of nonuniform composition is given by $f(c, \nabla c, \nabla^2 c, \ldots)$. We expand f in a multivariable Taylor series about $\mathbf{c}_0 = (c, 0, 0, \ldots)$. Then, we ignore the terms higher than second-order derivative terms.

$$\begin{aligned} &f(c, c_1, c_2, c_3, c_{11}, c_{22}, c_{33}, c_{12}, c_{23}, c_{31}, \ldots) \\ &= F(c) + \sum_i \frac{\partial f(\mathbf{c}_0)}{\partial c_i} c_i + \sum_{i,j=1}^{3} \frac{\partial f(\mathbf{c}_0)}{\partial c_{ij}} c_{ij} + \frac{1}{2}\sum_{i,j=1}^{3} \frac{\partial^2 f(\mathbf{c}_0)}{\partial c_i \partial c_j} c_i c_j \\ &\quad + \frac{1}{2}\sum_{i,j,k=1}^{3} \frac{\partial^2 f(\mathbf{c}_0)}{\partial c_k \partial c_{ij}} c_k c_{ij} + \frac{1}{2}\sum_{i,j,k,l=1}^{3} \frac{\partial^2 f(\mathbf{c}_0)}{\partial c_{ij} \partial c_{kl}} c_{ij} c_{kl} + \cdots, \end{aligned}$$

where c_1 and c_{12} denote the partial derivative by $\frac{\partial c}{\partial x_1}$ and $\frac{\partial^2 c}{\partial x_1 \partial x_2}$, respectively. For an isotropic medium, the free energy must be invariant to all rotations and reflections. Thus, the system is invariant to reflection $x_i \to -x_i$ and permutation $x_i \to x_j$ or x_k operations, and hence,

$$\frac{\partial f(\mathbf{c}_0)}{\partial c_i} = 0, \quad \frac{\partial f(\mathbf{c}_0)}{\partial c_{ii}} = \kappa_1, \quad \frac{\partial^2 f(\mathbf{c}_0)}{\partial c_i^2} = \kappa_2 \quad \text{for } i = 1, 2, 3,$$

$$\frac{\partial f(\mathbf{c}_0)}{\partial c_{ij}} = \frac{\partial^2 f(\mathbf{c}_0)}{\partial c_i \partial c_j} = 0 \quad \text{for } i \neq j.$$

That is, the free energy must be invariant to changes in the sign of the coordinate x. Then, we have

$$f(c, c_1, c_2, c_3, c_{11}, c_{22}, c_{33}, \ldots) = F(c) + \kappa_1 \Delta c + \frac{\kappa_2}{2}|\nabla c|^2 + \cdots.$$

We then integrate over the volume V of the solution to obtain the total free energy F of this volume:

$$\mathcal{E}(c) = N_V \int_\Omega f \mathrm{d}\mathbf{x} = N_V \int_\Omega \left[F(c) + \kappa_1 \Delta c + \frac{\kappa_2}{2}|\nabla c|^2 + \cdots\right] \mathrm{d}\mathbf{x}. \tag{13}$$

Integrating the second term on the right-hand side by parts and assuming the term $\partial c/\partial n$ vanishes at the boundary, we have

$$\begin{aligned} \int_\Omega \kappa_1 \Delta c \, \mathrm{d}\mathbf{x} &= \int_{\partial\Omega} \kappa_1 \frac{\partial c}{\partial n} \mathrm{d}\mathbf{s} - \int_\Omega \nabla \kappa_1 \cdot \nabla c \, \mathrm{d}\mathbf{x} = -\int_\Omega \sum_{i=1}^{3} \frac{\partial \kappa_1}{\partial x_i} \frac{\partial c}{\partial x_i} \mathrm{d}\mathbf{x} \\ &= -\int_\Omega \sum_{i=1}^{3} \frac{\partial \kappa_1}{\partial c} \left(\frac{\partial c}{\partial x_i}\right)^2 \mathrm{d}\mathbf{x} = -\int_\Omega \frac{\partial \kappa_1}{\partial c} |\nabla c|^2 \, \mathrm{d}\mathbf{x}. \end{aligned}$$

Thus, we can get

$$\begin{aligned} \mathcal{E}(c) &= N_V \int_\Omega f \, \mathrm{d}\mathbf{x} = N_V \int_\Omega \left[F(c) + \left(\frac{\kappa_2}{2} - \frac{\partial \kappa_1}{\partial c}\right)|\nabla c|^2 + \cdots\right] \mathrm{d}\mathbf{x} \\ &= N_V \int_\Omega \left[F(c) + \frac{\epsilon^2}{2}|\nabla c|^2 + \cdots\right] \mathrm{d}\mathbf{x}, \end{aligned} \tag{14}$$

where $\epsilon^2 = \kappa_2 - 2\partial\kappa_1/\partial c$. Eq. (14) is the central equation for the treatment. It reveals that through the first approximation, the free energy of a small volume of nonuniform solution can be expressed as the sum of two contributions, one being the free energy that this volume would have in a homogeneous solution, and the other, a gradient energy that is a function of the local composition. Thus, the CH equation is deduced from the Ginzburg–Landau free energy theory in units of N_V:

$$\mathcal{E}(c) \equiv \int_\Omega \left[F(c) + \frac{\epsilon^2}{2}|\nabla c|^2\right] \mathrm{d}\mathbf{x}. \tag{15}$$

To obtain the CH equation with variable mobility, one introduces a chemical potential μ as the variational derivative of $\mathcal{E}$,

$$\mu \equiv \frac{\delta \mathcal{E}}{\delta c} = F\prime(c) - \epsilon^2 \Delta c,$$

and defines the net flux of component B as $\mathcal{J} \equiv -M\nabla\mu$. Using a continuity equation, we have

$$\frac{\partial c}{\partial t} = -\nabla \cdot \mathcal{J},$$

which is the CH equation. The natural boundary condition and no-flux boundary conditions are

$$\nabla c \cdot \mathbf{n} = 0 \quad \text{and} \quad \mathcal{J} \cdot \mathbf{n} = 0 \text{ on } \partial\Omega, \tag{16}$$

where $\mathbf{n}$ is the unit normal vector to $\partial\Omega$. Then, we differentiate the energy $\mathcal{E}$ and the total mass $\int_\Omega c \, d\mathbf{x}$ to get

$$\begin{aligned} \frac{d}{dt}\mathcal{E}(t) &= \int_\Omega \left[F'(c)\frac{\partial c}{\partial t} + \epsilon^2 \nabla c \cdot \nabla \frac{\partial c}{\partial t}\right] \mathrm{d}\mathbf{x} = \int_\Omega \mu \frac{\partial c}{\partial t} \mathrm{d}\mathbf{x} \\ &= \int_\Omega \mu \nabla \cdot (M \nabla \mu) \mathrm{d}\mathbf{x} \\ &= \int_{\partial\Omega} \mu M \nabla \mu \cdot \mathbf{n} \, \mathrm{d}\mathbf{s} - \int_\Omega \nabla \mu \cdot (M \nabla \mu) \mathrm{d}\mathbf{x} \\ &= -\int_\Omega M |\nabla \mu|^2 \, \mathrm{d}\mathbf{x}, \end{aligned} \tag{17}$$

and

$$\frac{d}{dt}\int_\Omega c \, \mathrm{d}\mathbf{x} = \int_\Omega \frac{\partial c}{\partial t} \mathrm{d}\mathbf{x} = \int_\Omega M \Delta \mu \, \mathrm{d}\mathbf{x} = \int_{\partial\Omega} M \nabla \mu \cdot \mathbf{n} \, \mathrm{d}\mathbf{s} = 0,$$

where we used the no-flux boundary condition (16). Therefore, the total energy is non-increasing in time and the total mass is conserved.

Nevertheless, the thermodynamically free energy potential is given by (9), such a potential is often replaced with a polynomial of degree four for convenience (see Fig. 6). This is typically used for local minima such that

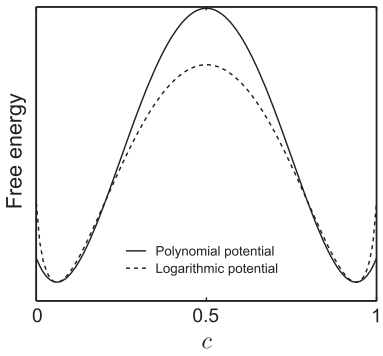

Fig. 6. A fourth polynomial is approximated to fit the positions of local minima of the logarithmic potential energy as well as the same curvatures at the points.

$$f(c) = \alpha(c-\beta)^2(c-\gamma)^2, \quad \alpha > 0 \text{ and } \gamma > \beta > 0.$$

This form of the double well free energy polynomial may approximate the one suggested by Cahn and Hilliard. We also note that both polynomial forms lead to a diffuse interface and have been studied from analytical, mathematical, and numerical viewpoints in previous studies [29–32].

3. Mathematical derivation

There are a number of different ways to derive the Cahn–Hilliard equation. For a gradient flow, this section is conceived in such a way that giving an intuitive understanding of the existence and uniqueness of the Cahn–Hilliard equation, and minimizing the functional theory for readers from many different research areas. We also mention several results of the equation with a brief historical survey of the field. Novick-Cohen and Segel [33] gave one of the first analyses to construct finite-amplitude equilibrium solutions in one dimensional space. Elliott and Songmu [30] proved existence of global solution in an L_2-setting for a constant mobility and polynomial free energy. For the existence result in the whole space, we refer to the work of Caffarelli and Muler [34]. The existence and uniqueness result for the double obstacle potential was shown by Blowey and Elliott [35], for logarithmic potentials with constant mobilities by Debussche and Dettori [36]. For a microforce balance, Miranville [37] proved the existence and uniqueness of solutions. The multicomponent equation for existence and uniqueness was also studied by Elliott and Luckhaus [38]. For the degenerate case in one dimensional case, existence theory was proved by Yin [39]. Later, Elliott and Garcke proved the existence of solutions for arbitrary space dimensions with degenerate mobility [40]. Based on asymptotic expansions, limiting behavior was analyzed by Pego [41] heuristically, and by Alikakos, Bates and Chen rigorously [42]. Further Otto [43] and Glasner [44] (and references therein) have demonstrated the relationship between Mullins–Sekerka dynamics and Cahn–Hilliard model. The logarithmically slow coarsening rate was investigated by Alikakos et al. [45]. Kohn and Otto [46] considered the constant-mobility and degenerate-mobility equations for coarsening rates. It should be noted that the equation can also be regarded as the gradient flow with the energy functional in Fife's works [47,48]. As for counting equilibria, Grinfeld and Novick-Cohen [49] proved in one dimensional case. In [50], Rybka and Hoffmann proved that solutions of the Cahn–Hilliard equation converge to equilibria in dimensions $d = 1$, 2 and 3. In [51], Wei and Winter constructed a boundary-spike-layer solution. Existence of solutions with logarithmic potentials and dynamic boundary conditions was given by Gilardi et al. [52], and asymptotic behavior with dynamic boundary conditions was considered by Wu and Zheng [53]. Chill, Fasangov, and Pruss showed that the convergence to steady states with dynamic boundary conditions in [54]. Now, we review the derivation of the CH equation as a gradient flow [48]. Let $\mathcal{E}$ be a real-valued functional in which the function v should satisfy $\int v(x)\mathrm{d}\mathbf{x} = 0$. Then, the gradient flow is a dynamical system with respect to the time t:

$$\frac{\partial c}{\partial t} = -\mathrm{grad}_0\mathcal{E}(c).$$

The symbol "grad_0" here represents the sense of the Gâteaux derivative on the mass-conserving space, where the function v satisfies the conditions (16). To find a constrained gradient flow of $\mathcal{E}$, we define an appropriate space. Thus, we have a Hilbert space H of functions such that

$$\frac{\mathrm{d}}{\mathrm{d}\theta}\mathcal{E}(c+\theta v)\Big|_{\theta=0} = \langle \mathrm{grad}_0\mathcal{E}(c), v\rangle.$$

The next task is to determine what is meant by $\mathrm{grad}_0\mathcal{E}(c)$. By constraining the total mass such that

$$\int_\Omega c(\mathbf{x},t)\mathrm{d}\mathbf{x} = \text{constant}, \tag{18}$$

we can choose the Hilbert subspace $\dot{H}$ as a zero average subspace $\int v(x)\mathrm{d}\mathbf{x} = 0$ and its bounded linear mapping $\dot{H}^{-1}$ on the zero average space. To obtain the equivalent inner product on a dense subspace of $v_1, v_2 \in \dot{H}^{-1}$, we use L^2 such that

$$(v_1, v_2)_{\dot{H}^{-1}} \equiv (\nabla\phi_{v_1}, \nabla\phi_{v_2})_{L^2}, \tag{19}$$

where $\phi_{v_1}, \phi_{v_2} \in \dot{H}^1$ are the associates of v_1, v_2. Then, ϕ_v have the Neumann boundary value problem such as

$$-\Delta\phi_v = v \quad \text{in } \Omega, \quad \frac{\partial\phi_v}{\partial n} = 0 \quad \text{on } \partial\Omega, \quad \text{and} \quad \int_\Omega \phi_v\,\mathrm{d}\mathbf{x} = 0. \tag{20}$$

To show the existence and uniqueness of solutions (20), we first define the bilinear functional B on $\dot{H}^1$, that is, $B : \dot{H}^1 \times \dot{H}^1 \to \mathbb{R}$, by

$$\begin{aligned} B[\phi_{v_1}, \phi_{v_2}] &= \int_\Omega \nabla\phi_{v_1}\cdot\nabla\phi_{v_2}\,\mathrm{d}\mathbf{x} \\ &\equiv (\nabla\phi_{v_1}, \nabla\phi_{v_2})_{L^2}, \quad \text{for any } \phi_{v_1}, \phi_{v_2} \in \dot{H}^1. \end{aligned}$$

Then, we prove energy estimates for the bilinear form $B[\phi_{v_1}, \phi_{v_2}]$. The boundedness of the bilinear functional can be shown by the Hölder inequality, and for certain constants $C > 0$,

$$|B[\phi_{v_1}, \phi_{v_2}]| \leqslant \|\nabla\phi_{v_1}\|_{L^2}\|\nabla\phi_{v_2}\|_{L^2} \leqslant C\|\phi_{v_1}\|_{\dot{H}^1}\|\phi_{v_2}\|_{\dot{H}^1}.$$

Thus, the bilinear map is bounded.

Next, we see that $B[\phi_{v_1}, \phi_{v_2}]$ is coercive. From the definition of $B[\phi_{v_1}, \phi_{v_2}]$, we have

$$\|\nabla\phi_{v_1}\|_{L^2}^2 = B[\phi_{v_1}, \phi_{v_1}] \quad \text{for any } \phi_{v_1} \in \dot{H}^1. \tag{21}$$

In addition to Eq. (20) in which $(\phi_{v_1})_\Omega = \int_\Omega \phi_{v_1}(x)\mathrm{d}\mathbf{x}/|\Omega|$, using the Poincare inequality, we obtain

$$\begin{aligned} \|\phi_{v_1}\|_{L^2}^2 &= \int_\Omega \phi_{v_1}^2\,\mathrm{d}\mathbf{x} = \int_\Omega (\phi_{v_1} - (\phi_{v_1})_\Omega)^2 \leqslant C\int_\Omega |\nabla\phi_{v_1}|^2\,\mathrm{d}\mathbf{x} \\ &= CB[\phi_{v_1}, \phi_{v_1}], \end{aligned}$$

where C depends on Ω. Combining this with (21),

$$\frac{1}{C+1}\|\phi_{v_1}\|_{\dot{H}^1}^2 \leqslant B[\phi_{v_1}, \phi_{v_1}]. \tag{22}$$

Further, we let $\phi_{v_2} \in \dot{H}^1$, and then define

$$F(\phi_{v_1}) = \int_\Omega v\phi_{v_1}\,\mathrm{d}\mathbf{x} \quad \text{for every } v \in \dot{H}^{-1}.$$

Since the functional is linear bounded on $\dot{H}^1$, we can now apply the Lax–Milgram theorem to obtain a unique $\phi_{v_1} \in \dot{H}^1$ such that $B[\phi_{v_1}, \phi_{v_2}] = F(\phi_{v_2})$ for all $\phi_{v_2} \in \dot{H}^1$.

Finally, we define grad_0 in as follows: let c be sufficiently smooth and satisfy $\partial c/\partial n = \partial \Delta c/\partial n = 0$ on $\partial\Omega$. Then, we have the following equations in the sense of the Gateaux differential for all $v \in \dot{C}_0^\infty$:

$$\begin{aligned}\langle \text{grad}_0 \mathcal{E}(c), v\rangle &= \frac{d}{d\theta}\mathcal{E}(c+\theta v)\Big|_{\theta=0} = \lim_{\theta\to 0}\frac{1}{\theta}[\mathcal{E}(c+\theta v)-\mathcal{E}(c)] \\ &= \int_\Omega [F'(c)-\epsilon^2\Delta c]\, v \, d\mathbf{x} \\ &= -\int_\Omega [F'(c)-\epsilon^2\Delta c]\Delta\phi_v \, d\mathbf{x} \\ &= \int_\Omega \nabla[F'(c)-\epsilon^2\Delta c]\cdot\nabla\phi_v \, d\mathbf{x} \\ &= (\nabla[F'(c)-\epsilon^2\Delta c], \nabla\phi_v)_{L^2} \\ &= (-\nabla\cdot\nabla[F\prime(c)-\epsilon^2\Delta c], -\nabla\cdot\nabla\phi_v)_{\dot{H}^{-1}} \\ &= (-\Delta[F'(c)-\epsilon^2\Delta c], v)_{\dot{H}^{-1}}. \end{aligned} \tag{23}$$

Here, we put $-\Delta\phi_v$ in place of the v term in Eq. (23) and integrate it by parts. Thus, in the last equation, $\nabla\phi_v$ has a zero normal component on $\partial\Omega$ and zero flux condition (16). We identify

$$\text{grad}_0 \mathcal{E}(c) \equiv -\Delta[F'(c)-\epsilon^2\Delta c], \tag{24}$$

and specify its domain as those functions in $\dot{H}^1$ where the condition is satisfied with Eq. (16). Finally, it yields the evolution equation such that

$$\frac{\partial c}{\partial t} = \triangle[F'(c)-\epsilon^2\triangle c], \tag{25}$$

which is known as the Cahn–Hilliard equation in the open and bounded subset of $\mathbb{R}^3$ with a C^1 boundary domain Ω.

4. Cahn–Hilliard solver

Since the CH equation is nonlinear, it is difficult to find a closed-form solution. Therefore, for most cases we have to resort to numerical approximations to the CH equation. The CH equation is solved numerically by applying several methods such as the finite difference, finite element, and Fourier-spectral methods, and their adaptations. Let us define an order parameter ϕ as the relative concentration difference $\phi = c_B - c_A$, where c_A and c_B denote the compositions of components A and B, respectively, i.e., $c_A + c_B = 1$. Using the previous notation, we have $\phi = 2c - 1$. Then, the CH equation can be rewritten as

$$\frac{\partial \phi}{\partial t} = \triangle[F'(\phi)-\epsilon^2\triangle\phi], \tag{26}$$

with the new definition of $F(\phi) = 0.25(\phi^2-1)^2$. We note that in a steady state, a closed-form solution is $\phi(x) = \tanh\left(\frac{x}{\sqrt{2}\epsilon}\right)$ in the whole space domain $(-\infty, \infty)$.

4.1. Finite difference method

We now present numerical methods in finite difference schemes. We shall first discretize the CH Eq. (26) in a two-dimensional space, $\Omega = (a, b)\times(c, d)$. One- and three-dimensional discretizations are analogously defined.

Let N_x and N_y be positive integers. For simplicity, we consider a uniform mesh, i.e., the size of the spatial step is $h = (b-a)/N_x = (d-c)/N_y$. Let a computational domain be partitioned in Cartesian geometry into a uniform mesh with spatial step h. We denote cell-centered points by $(x_i, y_j) = (a + (i-0.5)h,\ c + (j-0.5)h)$. Let ϕ_{ij}^n and μ_{ij}^n be approximations of $\phi(x_i, y_j, t_n)$ and $\mu(x_i, y_j, t_n)$, respectively, where $t_n = n\Delta t$ and Δt is the temporal step. We first implement the zero Neumann boundary condition (16) by requiring that

$$\phi_{0j} = \phi_{1j},\ \phi_{N_x+1,j} = \phi_{N_x,j},\ \phi_{i0} = \phi_{i1},\ \text{and}\ \phi_{i,N_y+1} = \phi_{i,N_y}.$$

In most studies, for both ϕ and μ, Neumann boundary conditions are used, which means that the interface is orthogonal to the boundary and that there is no mass flux at the boundary. The physical importance of the Dirichlet boundary problem is that it governs the propagation of a solidification front into an ambient medium that is at rest, relative to the front [55]. The periodic boundary is used for simulation in order to mimic a large system or to minimize the boundary effect. Du and Nicolaides [55] proposed a finite element scheme and a finite difference scheme whereby the total energy decreases with time under the Dirichlet boundary conditions.

We define discrete energy as

$$\mathcal{E}^h(\phi^n) = \sum_{i=1}^{N_x}\sum_{j=1}^{N_y}\left(h^2 F(\phi_{ij}^n) + \frac{\epsilon^2}{2}\left[(\phi_{i+1,j}^n-\phi_{ij}^n)^2 + (\phi_{i,j+1}^n-\phi_{ij}^n)^2\right]\right).$$

A fully implicit scheme for the CH equation was adopted by Chella and Viñals [56].

$$\frac{\phi_{ij}^{n+1}-\phi_{ij}^n}{\Delta t} = \Delta_d\left(F'(\phi_{ij}^{n+1}) - \epsilon^2\Delta_d\phi_{ij}^{n+1}\right),$$

where Δ_d is the standard discrete Laplacian.

A conservative nonlinear multigrid method for the CH equation with variable mobility was proposed in a previous study [57]. The method uses the standard finite difference approximation in spatial discretization and the Crank–Nicolson scheme in temporal discretization:

$$\begin{aligned}\frac{\phi_{ij}^{n+1}-\phi_{ij}^n}{\Delta t} &= \nabla_d\cdot\left[M(\phi)_{ij}^{n+\frac{1}{2}}\nabla_d\mu_{ij}^{n+\frac{1}{2}}\right], \quad \mu_{ij}^{n+\frac{1}{2}} \\ &= \frac{1}{2}\left(F'\left(\phi_{ij}^{n+1}\right)+F'\left(\phi_{ij}^n\right)\right) - \frac{\epsilon^2}{2}\Delta_d\left(\phi_{ij}^{n+1}+\phi_{ij}^n\right).\end{aligned}$$

Discrete versions of mass conservation and energy dissipation were proved.

Typically, one would prefer a temporal step restriction owing to accuracy requirements and not stability limitations [58]. In the CH equation, a discrete time-stepping algorithm is defined to be *unconditionally gradient stable* if

$$\mathcal{E}^h(\phi^{n+1}) \leqslant \mathcal{E}^h(\phi^n) \quad \text{for all } n, \tag{27}$$

holds for any size of the temporal step Δt [58]. We show the pointwise boundedness of the numerical solution under the condition (27). Let ϕ^n be a numerical solution satisfying (27) for a discrete CH equation. Let us assume that there does not exist a constant K for all n such that

$$\|\phi^n\|_\infty \leqslant K. \tag{28}$$

Then, there is an integer n_K dependent on K such that $\|\phi^{n_K}\|_\infty > K$ for each K, and an index $i (1 \leqslant i \leqslant N_x)$ such that $|\phi_i^{n_K}| > K$. Let $K = \sqrt{1+2\sqrt{\mathcal{E}^h(\phi^0)/h}}$, then, we have $\mathcal{E}^h(\phi^0) = hF(K) < hF(|\phi_i^{n_K}|) \leqslant \mathcal{E}^h(\phi^{n_K}) \leqslant \mathcal{E}^h(\phi^0)$. This contradiction implies that Eq. (28) should be satisfied [9].

Numerical solutions for non-linearly stabilized splitting schemes using a multigrid method can be found in a previous study [59]. The resulting equations are as follows:

$$\frac{\phi_{ij}^{n+1}-\phi_{ij}^n}{\Delta t} = \Delta_d v_{ij}^{n+1} - \Delta_d\phi_{ij}^n, \tag{29}$$

$$v_{ij}^{n+1} = F'(\phi_{ij}^{n+1}) + \phi_{ij}^{n+1} - \epsilon^2\Delta_d\phi_{ij}^{n+1}. \tag{30}$$

Bullard et al. [60] and Eyre [61] proved that the solutions of Eqs. (29) and (30) satisfy the inequality (27). Another candidate is the linearly stabilized splitting scheme. In this scheme, the nonlinear term $F'(\phi)$ is treated as a source term. Therefore, we solve a system of linear equations as follows:

$$\frac{\phi_{ij}^{n+1}-\phi_{ij}^{n}}{\Delta t}=\Delta_d v_{ij}^{n+1}+\Delta_d(F\prime(\phi_{ij}^{n})-2\phi_{ij}^{n}),\ v_{ij}^{n+1}=2\phi_{ij}^{n+1}-\epsilon^2\Delta_d\phi_{ij}^{n+1}.$$

Vollmayr-Lee and Rutenberg [58] applied the von Neumann linear stability analysis [62] to a class of numerical schemes.

Furihata et al. [63] examined the boundedness of the solution of a finite difference scheme [64] using a discretized Lyapunov functional. Furihata [65] proposed a stable and conservative finite difference scheme that inherits the properties of mass conservation and total energy decrease under a certain condition on Δt and h.

Many multiphase flow problems involve both small and large scales. In order to effectively resolve multiple scales, we need to consider adaptive grid refinement [66]. Krysl, Grinspun, and Schroder proposed a local adaptive refinement method (CHARMS) [67]. Another approach is adaptive mesh refinement (AMR) [68], in which the computational mesh is locally refined in regions where greater accuracy is desired (see Fig. 7 for an example of the grid structure) [69]. To generate the adaptive mesh, we tag cells that contain the interface. Using a clustering algorithm [70], the tagged cells are grouped into rectangular patches. These rectangular patches are refined to form the grids at the next level. We repeat this process until a specified maximum level is reached.

Ceniceros et al. [71] presented an efficient numerical methodology for the 3D computation of incompressible multi-phase flows described by conservative phase-field models. The numerical method employs adaptive mesh refinement (AMR) in concert with an efficient semi-implicit time discretization strategy and a linear multi-level multigrid to relax high-order stability constraints and to capture the flow's disparate scales at optimal cost. Only five linear solvers are needed per time-step. Their formulation is based on a new second-order accurate time integration algorithm. The fully discrete formulation inherits the main characteristics of conserved phase dynamics, namely, mass conservation and nonlinear stability with respect to the free energy. They also proposed an adaptive time-stepping version of the new time integration method.

4.2. Finite element method

For the Galerkin finite element method for the CH equation, refer to previous studies [30,72,73]. It was noted that the numerical implementation was based on the choice of the piecewise polynomial spline space. The solution possessing asymptotic behavior and spatial structure was also shown. On the other hand, solutions were analyzed using an energy-based Lyapunov functional with a second-order splitting method. Blowey and Elliott [74] carried out numerical analysis of a parabolic variational problem arising from a deep quench limit of a model for phase separation in a binary mixture. In addition, a finite element approximation was studied for two fully discrete schemes, and schemes possessing Lyapunov functionals were verified [75]. To discretize for the finite element method, the set of evolution equations are solved in a weak form with a semi-implicit time scheme. Thus, the weak form of the equations is given by

$$\left(\phi^{n+1}-\phi^{n},\psi\right)_{L^2(\Omega)}+\Delta t\left(M(\phi^{n})\nabla\mu^{n+1},\nabla\psi\right)_{L^2(\Omega)}=0,\quad\forall\psi\in H^1(\Omega),\tag{31}$$

$$\epsilon^2\left(\nabla\phi^{n+1},\nabla\psi\right)_{L^2(\Omega)}+\left(F\prime(\phi^{n+1})-\phi^{n}-\mu^{n+1},\psi\right)_{L^2(\Omega)}=0,\tag{32}$$

where $H^1(\Omega)$ is the standard Sobolev space of $L^2(\Omega)$ functions with the first derivative in $L^2(\Omega)$, and $(a,b)_{L^2(\Omega)}$ is the $L^2(\Omega)$ inner product.

Zhang and Wang [76] used a convexity-splitting scheme to discretize in the temporal variable and a nonconforming finite element method to discretize in spatial variables. The scheme preserved the mass conservation and energy dissipation properties of the original problem. Fernandino and Dorao [77] used the least squares spectral element method to solve the CH equation. Kay and Welford [78] adopted adaptive mesh refinement for solving the CH equation using the finite element method. They solved the equation by applying the non-linear Gauss–Seidel iteration and the multigrid method.

4.3. Spectral method

Chen and Shen [79] introduced a semi-implicit Fourier-spectral method for the CH equation with periodic boundary conditions.

$$\frac{\partial\tilde{\phi}(\mathbf{k},t)}{\partial t}=-|\mathbf{k}|\tilde{F}'(\phi)(\mathbf{k},t)-\epsilon^2\tilde{\phi}(\mathbf{k},t),\tag{33}$$

where $\mathbf{k}$ is a vector in the Fourier space, and $\tilde{\phi}(\mathbf{k},t)$ and $\tilde{F}\prime(\phi)(\mathbf{k},t)$ represent the Fourier transform of $\phi(\mathbf{x},t)$ and $F(\phi)(\mathbf{x},t)$, respectively. They treated the linear fourth-order operators implicitly and the non-linear terms explicitly.

$$(1+\Delta t\epsilon^2|\mathbf{k}|^4)\tilde{\phi}^{n+1}(\mathbf{k})=\tilde{\phi}^{n}(\mathbf{k})-\Delta t|\mathbf{k}|^2\tilde{F}\prime(\phi)(\mathbf{k}).\tag{34}$$

This scheme is first-order accurate in time. The accuracy in time can be improved by using higher-order semi-implicit schemes [79]. Zhu et al. [80] implemented a semi-implicit Fourier-spectral method for the variable-mobility CH equation with periodic boundary conditions. Liu and Shen [81] analyzed a semi-discrete Fourier-spectral method for the numerical approximation of a phase-field model for the mixture of two incompressible fluids and implemented a semi-implicit scheme for time discretization. To improve the effectiveness of a Fourier spectral method, many researchers have attempted to solve the phase-field equation by combining an adaptive moving mesh to construct a time-dependent mapping from the computational domain to the physical domain [82,83]. Shen and Yang [84] developed a moving mesh spectral method for the phase-field model of two phase flows with non-periodic boundary conditions. The method is based on a variational moving mesh PDE for the phase function, coupled with efficient semi-implicit treatments for advancing the mesh function, the phase function and the velocity and pressure in a decoupled manner.

Let us consider an unconditionally stable Fourier-spectral method for the following CH equation in two-dimensional space:

$$\begin{aligned}\frac{\partial\phi}{\partial t}(x,y,t)&=\Delta\left(\phi^3(x,y,t)-\phi(x,y,t)\right)\\&\quad-\epsilon^2\Delta^2\phi(x,y,t)\text{for}(x,y,t)\\&\in(0,L_x)\times(0,L_y)\times(0,T).\end{aligned}\tag{35}$$

The boundary condition is the homogeneous Neumann

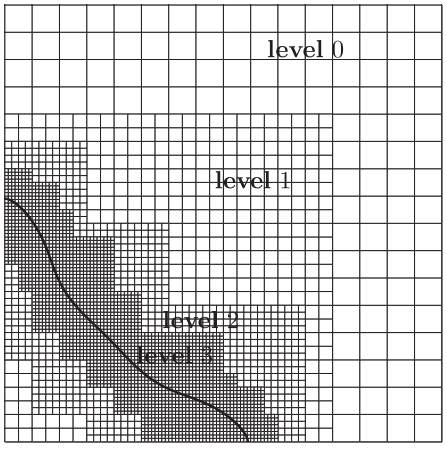

Fig. 7. Block-structured local refinement. In this example, there are four levels.

$$\frac{\partial \phi}{\partial x}(0,y,t) = \frac{\partial \phi}{\partial x}(L_x,y,t) = \frac{\partial \phi}{\partial y}(x,0,t) = \frac{\partial \phi}{\partial y}(x,L_y,t) = 0.$$

For the given data $\{\phi^k_{mn} | m = 1,\dots,M \text{ and } n = 1,\dots,N\}$, the discrete cosine transform is defined [85,86].

$$\hat{\phi}^k_{pq} = \alpha_p \beta_q \sum_{m=1}^{M}\sum_{n=1}^{N} \phi^k_{mn} \cos\frac{(2m-1)(p-1)\pi}{2M} \cos\frac{(2n-1)(q-1)\pi}{2N}, p = 1,\dots,M \quad \text{and} \quad q = 1,\dots,N,$$

where

$$\alpha_p = \begin{cases} \sqrt{1/M}, & p = 1 \\ \sqrt{2/M}, & 2 \leqslant p \leqslant M \end{cases} \quad \text{and} \quad \beta_q = \begin{cases} \sqrt{1/N}, & q = 1, \\ \sqrt{2/N}, & 2 \leqslant q \leqslant N. \end{cases}$$

For simplicity, we denote some variables by

$$x_m = \frac{(2m-1)L_x}{2M}, \quad y_n = \frac{(2n-1)L_y}{2N}, \quad \xi_p = \frac{p-1}{L_x}, \quad \eta_q = \frac{q-1}{L_y}.$$

By using these variables, we obtain the discrete cosine transform:

$$\hat{\phi}^k_{pq} = \alpha_p \beta_q \sum_{m=1}^{M}\sum_{n=1}^{N} \phi^k_{mn} \cos(x_m \pi \xi_p) \cos(y_n \pi \eta_q).$$

The inverse discrete cosine transform is

$$\phi^k_{mn} = \sum_{p=1}^{M}\sum_{q=1}^{N} \alpha_p \beta_q \hat{\phi}^k_{pq} \cos(\xi_p \pi x_m) \cos(\eta_q \pi y_n). \tag{36}$$

Let us assume that

$$\phi(x,y,k\Delta t) = \sum_{p=1}^{M}\sum_{q=1}^{N} \alpha_p \beta_q \hat{\phi}^k_{pq} \cos(\xi_p \pi x) \cos(\eta_q \pi y).$$

The x and y second-order partial derivatives translate into analytical differentiation of the exponentials.

$$\frac{\partial^2 \phi}{\partial x^2}(x,y,k\Delta t) = -\sum_{p=1}^{M}\sum_{q=1}^{N} (\xi_p \pi)^2 \alpha_p \beta_q \hat{\phi}^k_{pq} \cos(\xi_p \pi x) \cos(\eta_q \pi y),$$

$$\frac{\partial^2 \phi}{\partial y^2}(x,y,k\Delta t) = -\sum_{p=1}^{M}\sum_{q=1}^{N} \left(\eta_q \pi\right)^2 \alpha_p \beta_q \hat{\phi}^k_{pq} \cos(\xi_p \pi x) \cos(\eta_q \pi y).$$

Then, the Laplacian operator is defined as

$$\Delta\phi(x,y,k\Delta t) = -\sum_{p=1}^{M}\sum_{q=1}^{N} \left[(\xi_p \pi)^2 + \left(\eta_q \pi\right)^2\right] \alpha_p \beta_q \hat{\phi}^k_{pq} \cos(\xi_p \pi x) \times \cos(\eta_q \pi y).$$

We apply the linearly stabilized splitting scheme [61] to Eq. (35).

$$\frac{\phi^{k+1}_{ij} - \phi^k_{ij}}{\Delta t} = \Delta\left(2\phi^{k+1}_{ij} - \epsilon^2 \Delta \phi^{k+1}_{ij} + f(\phi^k_{ij})\right), \tag{37}$$

where $f(\phi) = \phi^3 - 3\phi$. Thus, Eq. (37) can be transformed into the discrete cosine space as follows:

$$\frac{\hat{\phi}^{k+1}_{pq} - \hat{\phi}^k_{pq}}{\Delta t} = -\left\{(\xi_p \pi)^2 + \left(\eta_q \pi\right)^2\right\}\left(2\hat{\phi}^{k+1}_{pq} + \epsilon^2 \left\{(\xi_p \pi)^2 + \left(\eta_q \pi\right)^2\right\} \hat{\phi}^{k+1}_{pq} + \hat{f}^k_{pq}\right).$$

Therefore, we obtain the following discrete cosine transform

$$\hat{\phi}^{k+1}_{pq} = \frac{\hat{\phi}^k_{pq} + A_{pq}\Delta t \hat{f}^k_{pq}}{1 - 2A_{pq}\Delta t + \epsilon^2 A^2_{pq}\Delta t}, \quad \text{where } A_{pq} = -\left\{(\xi_p \pi)^2 + (\eta_q \pi)^2\right\}. \tag{38}$$

The corresponding function ϕ^{k+1}_{mn} can be computed using Eq. (36). The following MATLAB script implements the scheme (37) using a spectral method [87]. Note that the presented code strongly follows the David Eyre's implemented MATLAB code [88].

```
clear all;xright = 2;yright = 1;M = 200;N = 100;
x = linspace(0.5*xright/M,xright-0.5*xright/M,M);
y = linspace(0.5*yright/N, yright-0.5*yright/N,N); h = x(2)-
   x(1);
[xx,yy]=meshgrid(x,y);dt = 0.1;maxiter = 500;epsilon = 4*h/
   (2*sqrt(2)*atanh(0.9));
xp = linspace(0,(M-1)/xright,M)'; yq = linspace(0,(N-1)/
   yright,N)';
Leig=-((xp.^2)*ones(1,N) + ones(M,1)*(yq'.^2))*pi*pi;
CHeig = ones(M,N)- 2*dt*Leig  + dt*epsilon^2*Leig.^2;
U = 0.001*(rand(M,N)-0.5); hat_U = dct2(real(U));
for it = 1:maxiter if rem(it,10)==0
subplot(2,1,1); surf(xx',yy',real(U))
shading interp; axis([0 xright 0 yright −1 1])
subplot(2,1,2); contourf(xx',yy',real(U), [-0.9 −0.45 0 0.35
   0.9])
axis image, axis([0 xright 0 yright]); getframe(gcf)
end
fU  = U.^3 - 3*U; hat_rhs  = hat_U  + dt*Leig.*dct2(real(fU));
hat_U  = hat_rhs./CHeig; U  = idct2(hat_U);
end
```

Using the above MATLAB [89] code, we examine the evolution of a random perturbation with small magnitude about a mean composition. For this purpose, the initial condition is taken to be $u(x, y, 0) = 0.01$ rand(x, y) in the computational domain $\Omega = (0,1) \times (0,1)$. Here rand$(x, y)$ is a random number between -1 and 1. We take the simulation parameters as $\epsilon = 0.005$, $h = 0.0026$, and $\Delta t = 0.01$. Here, ϵ is related to the interface thickness, given by $\epsilon_m = hm/[2\sqrt{2}\tanh^{-1}(0.9)]$ for the interface thickness with m grid points from the approximated solutions [90]. In Fig. 8, the four snapshots represent the temporal evolutions of morphological patterns during spinodal decomposition.

Now we perform the accuracy and efficiency test of the spectral method for the CH equation. Let us first analyze the accuracy of the scheme. The computations are performed on a unit square domain Ω up to time $T = 0.001$ with $\epsilon = 0.01$. Neumann boundary conditions are used. The initial condition is given as

$$\phi(x,y,0) = 0.03\cos(2\pi x)\cos(2\pi y) + 0.01\cos(\pi x)\cos(3\pi y).$$

We take the spatial step size $h = 1/2^n$, $n = 5, 6, 7, 8, 9$ and the temporal step size $\Delta t = 0.1024 \times h^2$. We define the error as the discrete l_2-norm of the difference between that grid and the average of the next finer grid cells:

$$e_{h/\frac{h}{2}ij} \overset{\text{def}}{=} \phi_{hij} - \left(\phi_{\frac{h}{2}2i,2j} + \phi_{\frac{h}{2}2i-1,2j} + \phi_{\frac{h}{2}2i,2j-1} + \phi_{\frac{h}{2}2i-1,2j-1}\right)\Big/4.$$

Then, the rate of convergence is defined as $\log_2\left(\|e_{h/\frac{h}{2}}\|/\|e_{\frac{h}{2}/\frac{h}{4}}\|\right)$. Table 1 shows that the scheme is first order accurate in time and second order accurate in space.

Next we present the efficiency test. Eq. (38) can be computed in $O(N \ln N)$ operations with the 2D Fast Cosine Transform [89,91,92]. Here N is the number of unknowns. We take the same parameters and initial condition in the above accuracy test except $\Delta t = 0.001$, $T = 1$, and $\epsilon = 4h/(2\sqrt{2}\tanh^{-1}(0.9))$. Fig. 9 shows the CPU time against the number of unknowns. Numerical results (circled symbols) are in good agreement with the best fit with $O(N \ln N)$ (solid line).

Finally, we present a model problem that has been used for testing the solvers. The problem is a phase separation test, which shows mass conservation and total energy decrease. The initial condition is $\phi(x, y, 0) = 0.1 + 0.1$ rand(x, y) on the unit domain with $\Delta t = 0.1$, $h = 1/128$, and $\epsilon = 4h/(2\sqrt{2}\tanh^{-1}(0.9))$. Fig. 10 shows the normalized discrete total energy $E(t)/E(0)$ (solid line) and average

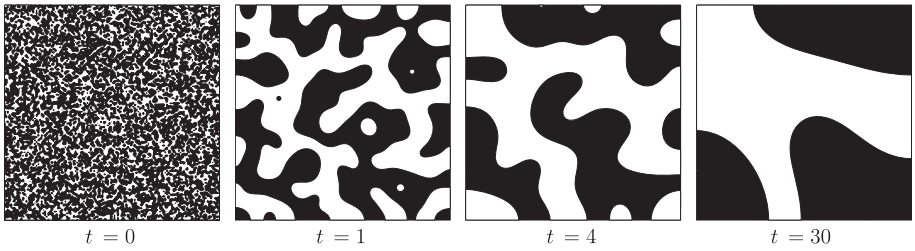

Fig. 8. Temporal morphological evolutions at different values of t.

Table 1
l_2-Norm of the errors and convergence rates of the scheme.

Case	32–64	Rate	64–128	Rate	128–256	Rate	256–512
l_2	2.18e−05	2.02	5.36e−06	2.01	1.33e−06	2.00	3.33e−07

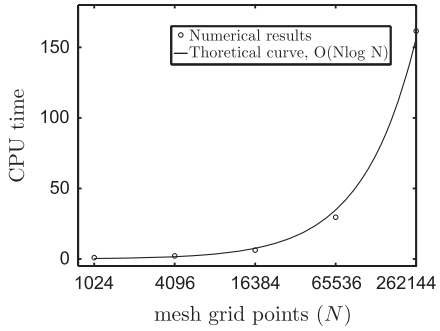

Fig. 9. CPU times against grid points N.

concentration (dashed line), which demonstrate the total energy dissipation and the mass conservation properties. The inscribed small figures are the snapshots at the indicated times (see Table 2).

The main challenges for solving the CH equation are resolving the relatively thick interfacial region and highly nonlinear equation. In real physics, the interfacial thickness is very small, i.e., 1 nm [107]. This small resolution cannot be resolved by current computational power. This small size limitation has been resolved partially by adaptive mesh refinement and parallel algorithms. The CH equation is a fourth-order nonlinear equation. Standard numerical discretizations have limitations in stability and solvability. These constraints have been solved by unconditionally stable schemes. The remaining challenges in this area are efficient and accurate parallel algorithms, unconditionally stable high-order temporal discretization, dynamic boundary condition, and rigorous

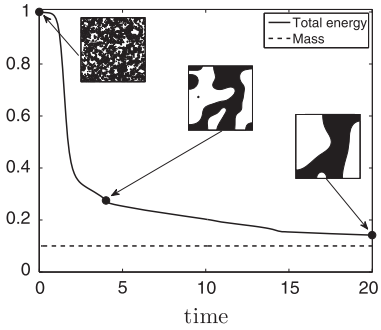

Fig. 10. Non-increasing discrete total energy and conservation of mass concentration.

Table 2
Previous studies for numerical methods.

- Galerkin finite element method [30,72]
- Second order splitting method [73]
- Nonconforming finite element method [93]
- Dirichlet boundary condition [55]
- Numerical analysis with a logarithmic free energy [29]
- Unconditionally gradient stable scheme [61]
- Semi-implicit Fourier-spectral method [79,94]
- With degenerate mobility [95]
- Stable and conservative finite difference scheme [65]
- Conservative multigrid method [96]
- Numerical solution with generic boundary condition [97]
- Discontinuous Galerkin method [98]
- Moving mesh [82]
- Adaptive mesh refinement [99]
- Local discontinuous Galerkin method [100]
- Large time-stepping method [101]
- Isogeometric analysis [102]
- Conservative scheme with contact angle boundary condition [103]
- Conservative scheme with Neumann bd. in complex domain [104]
- Conservative scheme with Dirichlet boundary in complex domain [105]
- Parallel multigrid method [106]

validation of the morphology evolution from the CH equation with that of experiment, to list a few.

5. Conclusions

In this article, we reviewed physical, mathematical, and numerical derivations of the binary CH equation. First, we described the physical derivation from the basic thermodynamics. We defined the chemical potential as the variational derivative of the total energy and its flux as the minus gradient of the potential. Using the usual continuity equation, we obtained the CH equation. Second, we outlined the mathematical derivation of the CH equation. Third, various numerical methods such as the finite difference, finite element, and spectral methods were discussed. We also provided a short MATLAB program code for the CH equation using a pseudo-spectral method.

Acknowledgments

The first author (D. Lee) was supported by Basic Science Research Program through the National Research Foundation of Korea (NRF) funded by the Ministry of Education, Science and Technology (No. 2013003181), and J.Y. Huh was supported by a grant from the Fundamental R&D Program for Core Technology of Materials funded by the Ministry of Knowledge Economy, Republic of Korea. The corresponding author (J.S. Kim) would like to thank Professor Kyungkeun Kang for helpful conversations on the theoretical part. The authors are grateful to the anonymous referees whose valuable suggestions and comments significantly improved the quality of this paper.

References

[1] J.W. Cahn, J.E. Hilliard, J. Chem. Phys. 28 (1958) 258–267.
[2] J.W. Cahn, J. Chem. Phys. 42 (1965) 93–99.
[3] P. Colli, G. Gilardi, P. Podio-Guidugli, J. Sprekels, SIAM J. Appl. Math. 71 (2011) 1849–1870.
[4] D. Anders, K. Weinberg, Comput. Mater. Sci. 50 (2011) 1359–1364.
[5] J.M. Park, R. Mauric, P.D. Anderson, Chem. Eng. Sci. 80 (2012) 270–278.
[6] F. Boyer, Comput. Fluids 31 (2002) 41–68.
[7] V.V. Khatavkar, P.D. Anderson, H.E.H. Meijer, Chem. Eng. Sci. 61 (2006) 2364–2378.
[8] J. Kim, J. Comput. Phys. 204 (2005) 784–804.
[9] J. Kim, Commun. Comput. Phys. 12 (2012) 613–661.
[10] H. Ganapathy, E. Al-Hajri, M.M. Ohadi, Chem. Eng. Sci. 94 (2013) 156–165.
[11] C. Zhou, S. Kumar, Chem. Eng. Sci. 81 (2012) 38–45.
[12] D. Molin, R. Mauri, Chem. Eng. Sci. 63 (2008) 2402–2407.
[13] D. Anders, C. Hesch, K. Weinberg, Int. J. Solids Struct. 49 (2012) 1557–1572.
[14] T.L. Tran, P.K. Chan, D. Rousseau, Chem. Eng. Sci. 60 (2005) 7153–7159.
[15] L.Q. Chen, Annu. Rev. Mater. Res. 32 (2002) 113–140.
[16] R. Ghoncheh, D.R. Alejandro, Chem. Eng. Sci. 71 (2012) 18–31.
[17] S.Y. Hu, L.Q. Chen, Acta. Mater. 49 (2001) 1879–1890.
[18] F. Marra, Chem. Eng. Sci. 71 (2012) 39–45.
[19] W. Gaudig, Comput. Mater. Sci. 77 (2013) 182–188.
[20] M. Mamivand, M.A. Zaeem, H.E. Kadiri, Comput. Mater. Sci. 77 (2013) 304–311.
[21] M.A. Zaeem, H.E. Kadiri, P.T. Wang, M.F. Horstemeyer, Comput. Mater. Sci. 50 (2011) 2488–2492.
[22] L. Zhang, M.R. Tonks, P.C. Millett, Y. Zhang, K. Chockalingam, B. Biner, Comput. Mater. Sci. 56 (2012) 161–165.
[23] A.L. Bertozzi, S. Esedoglu, A. Gillette, Multiscale Model. Simul. 6 (2007) 913–936.
[24] A.L. Bertozzi, S. Esedoglu, A. Gillette, IEEE Trans. Image Process. 16 (2007) 285–291.
[25] V. Cristini, X. Li, J. Lowengrub, S.M. Wise, J. Math. Biol. 58 (2009) 723–763.
[26] S.M. Wise, J. Lowengrub, H.B. Frieboes, V. Cristini, J. Theor. Biol. 253 (2008) 524–543.
[27] D.R. Gaskell, Introduction to the Thermodynamics of Materials, Taylor and Francis, New York, 2003.
[28] D.A. Porter, K.E. Easterling, Phase Transformations in Metals and Alloys, van Nostrand Reinhold, New York, 1993.
[29] M.I.M. Copetti, C.M. Elliott, Numer. Math. 63 (1992) 39–65.
[30] C.M. Elliott, Z. Songmu, Arch. Rational Mech. Anal. 96 (1986) 339–357.
[31] J. Lowengrub, L. Truskinovsky, Proc. Roy. Soc. London A 454 (1998) 2617–2654.
[32] W. Wahl, Math. Math. Eng. (delft Progrss report) 10 (1985) 291–310.
[33] A. Novick-Cohen, L.A. Segal, Physica D. 10 (1984) 277–298.
[34] L.A. Caffarelli, N.E. Muler, Arch. Rational Mech. Anal. 133 (1995) 129–144.
[35] J.F. Blowey, C.M. Elliott, Eur. J. Appl. Math. 2 (1991) 233–279.
[36] A. Debussche, L. Dettori, Nonlinear Anal.-Theor. 24 (1995) 1491–1514.
[37] A. Miranville, J. Appl. Math. 4 (2003) 165–185.
[38] C.M. Elliott, S. Luckhaus, IMA Preprint Series 887 (1991).
[39] J. Yin, J. Differ. Eqs. 97 (1992) 310–327.
[40] C.M. Elliott, H. Garcke, SIAM J. Numer. Anal. 27 (1996) 404–423.
[41] R.L. Pego, Proc. Roy. Soc. London A 422 (1989) 261–278.
[42] N.D. Alikakos, P.W. Bates, X. Chen, Arch. Ration. Mech. Anal. 128 (1994) 165–205.
[43] F. Otto, Arch. Ration. Mech. Anal. 141 (1998) 63–103.
[44] K. Glasner, Nonlinearity 16 (2003) 49–66.
[45] N.D. Alikakos, P.W. Bates, G. Fusco, J. Differ. Eqs. 90 (1991) 81–135.
[46] R.V. Kohn, F. Otto, Commun. Math. Phys. 229 (2002) 375–395.
[47] P.C. Fife, Dynamical Aspects of the Cahn–Hilliard Equations, University of Tennessee, Knoxville, TN, Barret Lectures, 1991.
[48] P.C. Fife, Electron. J. Differ. Eq. Conf. 48 (2000) 1–26.
[49] M. Grinfeld, A. Novick-Cohen, Proc. Roy. Soc. Edinb. A 125 (1995) 351–370.
[50] P. Rybka, K.H. Hoffmann, Commun. Partial Differen. Eqs. 24 (1999) 1055–1077.
[51] J. Wei, M. Winter, Ann. Inst. Henri Poincaré (C) Non Linear Anal. 15 (1998) 459–492.
[52] L. Gilardi, A. Miranville, G. Schimperna, Commun. Pure Appl. Anal. 8 (2009) 881–912.
[53] H. Wu, S. Zheng, J. Differ. Eqs. 204 (2004) 511–531.
[54] R. Chill, E. Fasangová, J. Prüess, Math. Nachr. 279 (2006) 1448–1462.
[55] Q. Du, R.A. Nicolaides, SIAM J. Numer. Anal. 28 (1991) 1310–1322.
[56] R. Chella, J. Viñals, Phys. Rev. E. 53 (1996) 3832–3840.
[57] J. Kim, Commun. Nonlinear. Sci. Numer. Simul. 12 (2007) 1560–1571.
[58] B.P. Vollmayr-Lee, A.D. Rutenberg, Phys. Rev. E. 68 (2003) 066703-1–066703-13.
[59] J. Kim, H.O. Bae, J. Korean Phys. Soc. 53 (2008) 672–679.
[60] J.W. Bullard, L.Q. Chen, R.K. Kalia, A.M. Stoneham, Computational and Mathematical Models of Microstructural Evolution, The Material Research Society, Warrendale, 1998.
[61] D.J. Eyre, Unconditionally gradient stable time marching the Cahn–Hilliard equation, in: Materials Research Society Symposium, vol. 529, 1998.
[62] W.H. Press, S.A. Teukolsky, W.T. Vetterling, B.P. Flannery, Numerical Recipes in C, Cambridge University Press, New York, 1993.
[63] D. Furihata, T. Onda, M. Mori, GAKUTO Int. Ser. Math. Sci. Appl. 2 (1993) 347–358.
[64] M. Dehghan, Math. Compt Simul. 71 (2006) 16–30.
[65] D. Furihata, Numer. Math. 87 (2001) 675–699.
[66] E. Uzgoren, J. Sin, W. Shyy, Commun. Comput. Phys. 5 (2009) 1–41.
[67] F. Boyer, C. Lapuerta, S. Minjeaud, B. Piar, M. Quintard, Transp. Porous Med. 82 (2009) 463–483.
[68] A.S. Almgren, J.B. Bell, P. Colella, L.H. Howell, M.L. Welcome, J. Comput. Phys. 142 (1998) 1–46.
[69] D.F. Martin, P. Colella, M. Anghel, F.L. Alexander, Comput. Sci Eng. 7 (2005) 24–31.
[70] M.J. Berger, I. Rigoustsos, An Algorithm for Point Clustering and Grid Generation, Tech. Report NYU-501, New York University-CIMS, 1991.
[71] H.D. Ceniceros, R.L. Nos, A.M. Roma, J. Comput. Phys. 229 (2010) 6135–6155.
[72] C.M. Elliott, D.A. French, IMA J. Appl. Math. 38 (1987) 97–128.
[73] C.M. Elliott, D.A. French, F.A. Milner, Numer. Math. 54 (1989) 575–590.
[74] J.F. Blowey, C.M. Elliott, Eur. J. Appl. Math. 3 (1992) 147–179.
[75] C.M. Elliott, The Cahn–Hilliard model for the kinetics of phase separation, in: J.F. Rodrigues (Ed.), Mathematical Models for Phase Change Problems, Internat. Ser. Numer. Math., vol. I88, 1989, pp. 35–73.
[76] S. Zhang, M. Wang, J. Comput. Phys. 229 (2010) 7361–7372.
[77] M. Fernandino, C.A. Dorao, Appl. Math. Model. 35 (2011) 797–806.
[78] D. Kay, R. Welford, J. Comput. Phys. 212 (2006) 288–304.
[79] L.Q. Chen, J. Shen, Comput. Phys. Commun. 108 (1998) 147–158.
[80] J. Zhu, L.Q. Chen, J. Shen, V. Tikare, Phys. Rev. E. 60 (1999) 3564–3572.
[81] C. Liu, J. Shen, Physica D 179 (2003) 211–228.
[82] W.M. Feng, P. Yu, S.Y. Hu, Z.K. Liu, Q. Du, L.Q. Chen, J. Comput. Phys. 220 (2006) 498–510.
[83] W.M. Feng, P. Yu, S.Y. Hu, Z.K. Liu, Q. Du, L.Q. Chen, Commun. Comput. Phys. 5 (2009) 582–599.
[84] J. Shen, X. Yang, J. Comput. Phys. 228 (2009) 2978–2992.
[85] N. Ahmed, T. Natarajan, K.R. Rao, IEEE Trans. Comput. C-23 (1974) 90–93.
[86] A.K. Jain, Proc. IEEE 69 (1981) 349–389.
[87] S.I. Khayam, The Discrete Cosine Transform: Theory and Application, Technical Report, Michigan State University, 2003.
[88] D. Eyre's Home Page, 2013. <http://www.math.utah.edu/~eyre/computing/matlab-intro/ch.txt>.
[89] MATLAB Version, The MathWorks, Massachusetts, USA, 2009.
[90] K.E. Teigen, X. Li, J. Lowengrub, F. Wang, A. Voigt, Commun. Math. Sci. 4 (2009) 1009–1037.
[91] D.L. Jones, Digital Signal Processing: A User's Guide, Connexions, Rice University, Houston, Texas, 2006.
[92] K.R. Rao, P.C. Yip, The Transform and Data Compression Handbook, CRC Press LLC, Boca Raton, 2001.
[93] C.M. Elliott, D.A. French, SIAM J. Numer. Anal. 26 (1989) 884–903.
[94] J. Shen, V. Tikare, Phys. Rev. E 60 (1999) 3565–3572.
[95] J.W. Barrett, J.F. Blowey, H. Garcke, SIAM J. Numer. Anal. 37 (1999) 286–318.
[96] J. Kim, K. Kang, J. Lowengrub, J. Comput. Phys. 19 (2004) 511–543.
[97] R. Kenzler, F. Eurich, P. Maass, B. Rinn, J. Schropp, E. Bohl, W. Dieterich, Comput. Phys. Commun. 133 (2001) 139–157.
[98] G.N. Wells, E. Kuhl, K. Garikipati, J. Comput. Phys. 218 (2006) 860–877.
[99] S.M. Wise, J. Kim, J. Lowengrub, J. Comput. Phys. 226 (2007) 414–446.
[100] Y. Xia, Y. Xu, C.-W. Shu, J. Comput. Phys. 227 (2007) 472–491.
[101] Y. He, Y. Liu, T. Tang, Appl. Numer. Math. 57 (2007) 616–628.
[102] H. Gómez, V.M. Calo, Y. Bazilevs, T.J.R. Hughes, Comput. Methods Appl. Mech. Eng. 197 (2008) 4333–4352.
[103] H.G. Lee, J. Kim, Comput. Fluids 44 (2011) 178–186.
[104] J. Shin, D. Jeong, J. Kim, J. Comput. Phys. 230 (2011) 7441–7455.
[105] Y. Li, D. Jeong, J. Shin, J. Kim, Comput. Math. Appl. 65 (2013) 102–115.
[106] J. Shin, S. Kim, D. Lee, J. Kim, Comput. Mater. Sci. 71 (2013) 89–96.
[107] D. Jacqmin, Contact-line dynamics of a diffuse fluid interface, J. Fluid Mech. 402 (2000) 57–88.